Supplementary Information

An efficient WS_2/Ni_3S_2 monolithic electrode for the hydrogen evolution reaction at industrial current densities

Huifang Wei [a, 1], Denghui Ma [a, 1], Guomin Li [c], Wangwang Zhang [c], Shiyao Cao [b, *], Jianming Li [a, *]

a School of New Energy, Ningbo University of Technology, Ningbo, 315211, China
b PetroChina Shenzhen New Energy Research Institute Co., LTD. Shenzhen 518052, China
c Collaborative Innovation Center of Chemistry for Energy Materials, College of Chemistry and Chemical Engineering, Xiamen University, Xiamen 361005, China
[*] *Corresponding Authors.*
E-mail addresses: jmli@nbut.edu.cn (Jianming Li), csy123@petrochina.com.cn (Shiyao Cao).
[1] These authors contributed equally to this work.

Preparation of the $2WS_2/Ni_3S_2$-NF catalyst.

Ammonium tungstate ($(NH_4)_{10}W_{12}O_{41}$~xH_2O), potassium hydroxide (KOH, AR), and thiourea were obtained from Sinopharm chemical reagent Co., Ltd. All chemicals were used without further purification. For the preparation of $2WS_2/Ni_3S_2$-NF catalyst, 40 mg $(NH_4)_{10}W_{12}O_{41}$~xH_2O and 20 mg thiourea were dispersed in 600 μL deionized water. Afterward, the solution was cautiously added on the surface of nickel foam (NF, 1 cm ×1 cm) drop by drop. And then, the decorated NF was transferred into a CVD furnace and annealed at 400 ℃ for 4 h with a temperature ramping rate of 10 ℃ min^{-1} under 50% H_2 and 50% Ar atmosphere. The monolithic catalyst WS_2/Ni_3S_2-NF was prepared. The Ni_3S_2 was synthesized via the same method except for the absence of $(NH_4)_{10}W_{12}O_{41}$~xH_2O. When the mass of $(NH_4)_{10}W_{12}O_{41}$~xH_2O is 20, 40 and 60 mg respectively, the catalysts are labeled as $1WS_2/Ni_3S_2$-NF, $2WS_2/Ni_3S_2$-NF and $3WS_2/Ni_3S_2$-NF. Pt/C-NF catalyst was prepared by dropping aqueous solution containing 10 mg commercial 20% Pt/C onto NF.

Materials characterizations.

The scanning electron micrograph (SEM) was performed on the ZEISS Sigma at 20 kV. High-resolution transmission electron microscopy (HRTEM) was performed by using the FEI Tecnai F20 microscope at an accelerating voltage of 200 kV. X-ray diffraction (XRD) was performed on SmartLab-SE XRD at 40 kV and 30 mA using Cu Kα radiation (λ=1.5418 Å) at a scan rate of 10 degrees per minute. Raman spectra were collected using 532 nm laser excitation with a beam size of ~1 μm (Horiba LabRAB HR800, Japan). X-ray photoelectron spectroscopy (XPS) data was acquired with PHI Quantera-2000.

Electrochemical measurements.

Electrochemical measurements were performed on CHI 760 electrochemical workstations in three-electrode or two-electrode systems in 1 M or 6 M KOH at 25 or 85 ℃. In the HER process, nickel foam and Hg/HgO electrode were used as counter and reference electrodes, respectively. The $2WS_2/Ni_3S_2$-NF electrode was a working electrode. In the water electrolysis process, both the working and counter electrodes were $2WS_2/Ni_3S_2$-NF electrodes. Linear sweep voltammetry (LSV) curves were collected in 1 M or 6 M KOH at 25 or 85 ℃ with the scan rate of 10 mV s^{-1} at the atmosphere of Ar by 85% *iR* compensation. Nyquist measurements were performed

with a frequency from 10^{-1} to 10^{5} Hz at open circuit potential in 1.0 M KOH solution at 25 ℃. The cyclic voltammograms (CVs) were tested in the range of 0.2 to 0.3 V *vs.* RHE at different rates from 20 to 180 mV s^{-1} in 1.0 M KOH solution at 25 ℃. The chronopotentiometry was tested at 1000 mA cm^{-2}. All the potentials were recorded with respect to the reversible hydrogen electrode (RHE): $E_{RHE} = E_{Hg/HgO} + 0.098 + 0.059$ pH. When both cathode and anode were $2WS_2/Ni_3S_2$-NF, it was denoted as $2WS_2/Ni_3S_2$-NF (+, -).

Theoretical Calculations.

All density functional theory (DFT) calculations were performed through the Vienna abinitio simulation package (VASP) [1]. The projection-augmented wave (PAW) method was used to explain the interaction between ions and electrons. The exchange and correlation energies were evaluated by the generalized gradient approximation (GGA) with Perdew-Burke-Ernzerhof (PBE) functional [2]. A cutoff kinetic energy of 400 eV in the plane-wave expansion and Monkhorst-Pack grids were set up 2×2×1 for WS_2 related surface systems and 2×3×1 for Ni_3S_2 related surface systems, respectively. The vacuum layer of 15 Å was set to prevent the interaction between the images along the z direction. Free energy change ΔG of the reaction was calculated by the following equation:

$$\Delta G = \Delta E + \Delta E_{ZPE} - T\Delta S$$

Where ΔE represents the electron energy difference from DFT calculations, ΔE_{ZPE} is the zero-point energy change of surface model systems, and ΔS represents the entropy change. The value of $\Delta E_{ZPE} - T\Delta S$ is about 0.24 V [3], so $\Delta G = \Delta E + 0.24$ eV. Add dipole corrections along the z direction to obtain correct forces. The van der Waals correction was considered for the weak interaction via using the DFT+D3 method of Grimme [4]. Furthermore, Bader charge analyses [5] were performed for Ni_3S_2(110) and W-doped Ni_3S_2(110) surfaces.

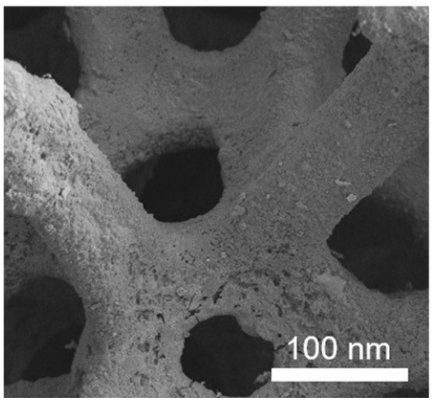

Supplementary Fig. 1 The SEM image of the $2WS_2/Ni_3S_2$-NF catalyst.

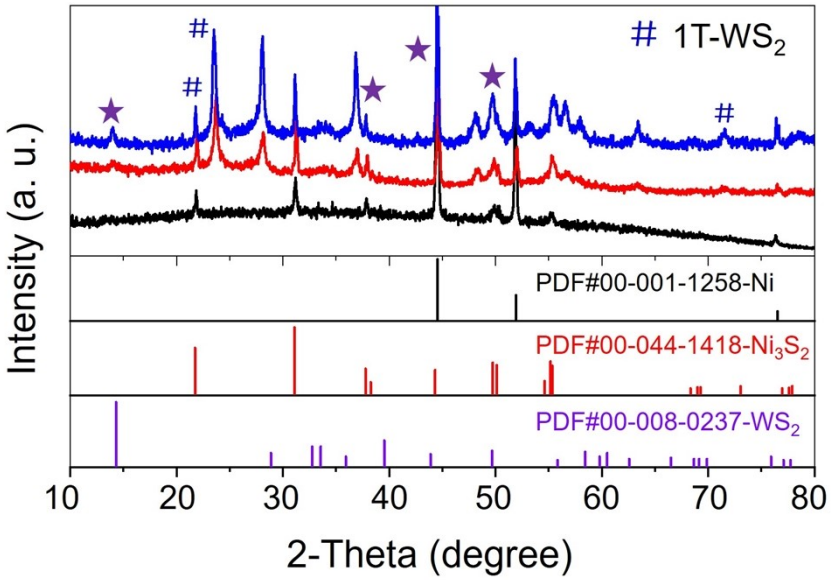

Supplementary Fig. 2 XRD analysis of the $1WS_2/Ni_3S_2$-NF (black), $2WS_2/Ni_3S_2$-NF (red) and $3WS_2/Ni_3S_2$-NF (blue) catalysts.

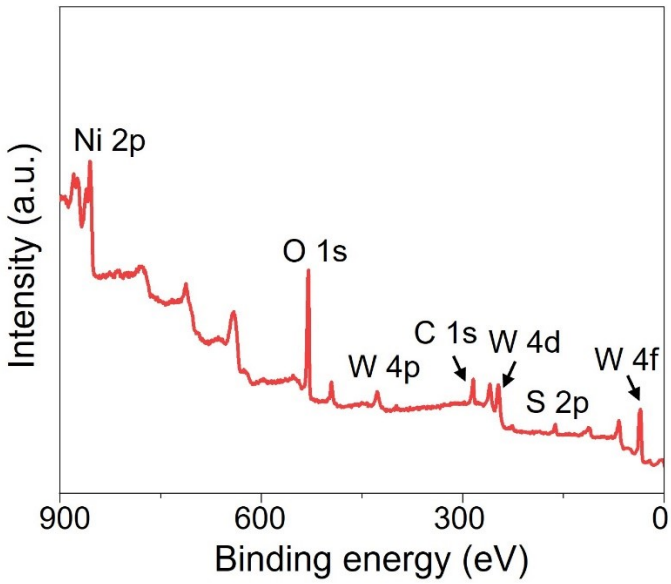

Supplementary Fig. 3 XPS survey spectrum of $2WS_2/Ni_3S_2$-NF catalyst.

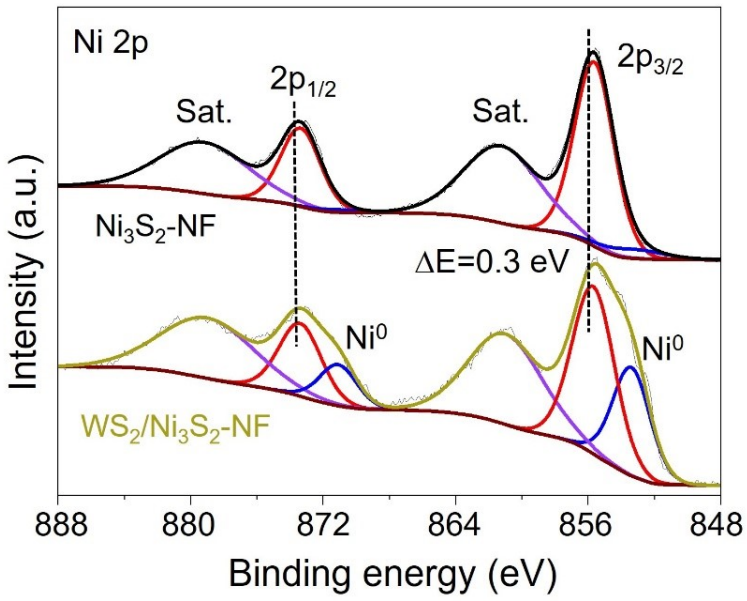

Supplementary Fig. 4 XPS spectra of WS_2/Ni_3S_2-NF and Ni_3S_2-NF catalysts for Ni 2p.

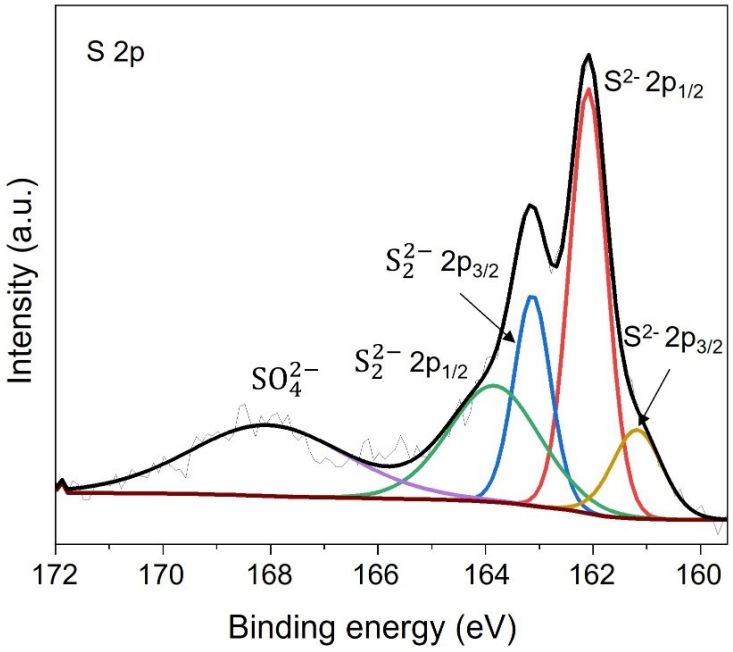

Supplementary Fig. 5 XPS spectra of WS_2/Ni_3S_2-NF catalyst for S 2p.

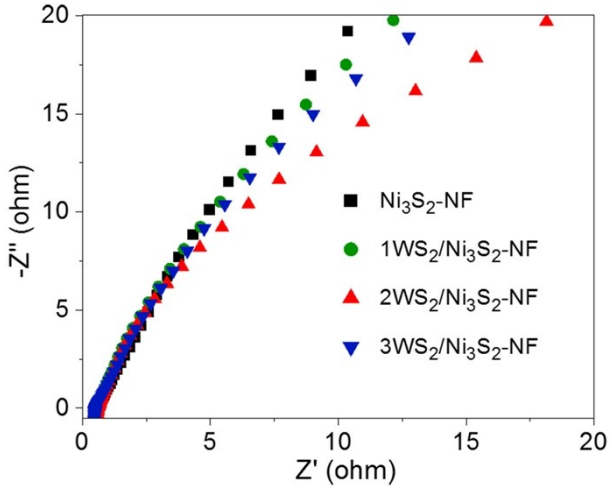

Supplementary Fig. 6 The electrochemical impedance spectroscopy of Ni_3S_2-NF, $1WS_2/Ni_3S_2$-NF, $2WS_2/Ni_3S_2$-NF, $3WS_2/Ni_3S_2$-NF catalysts.

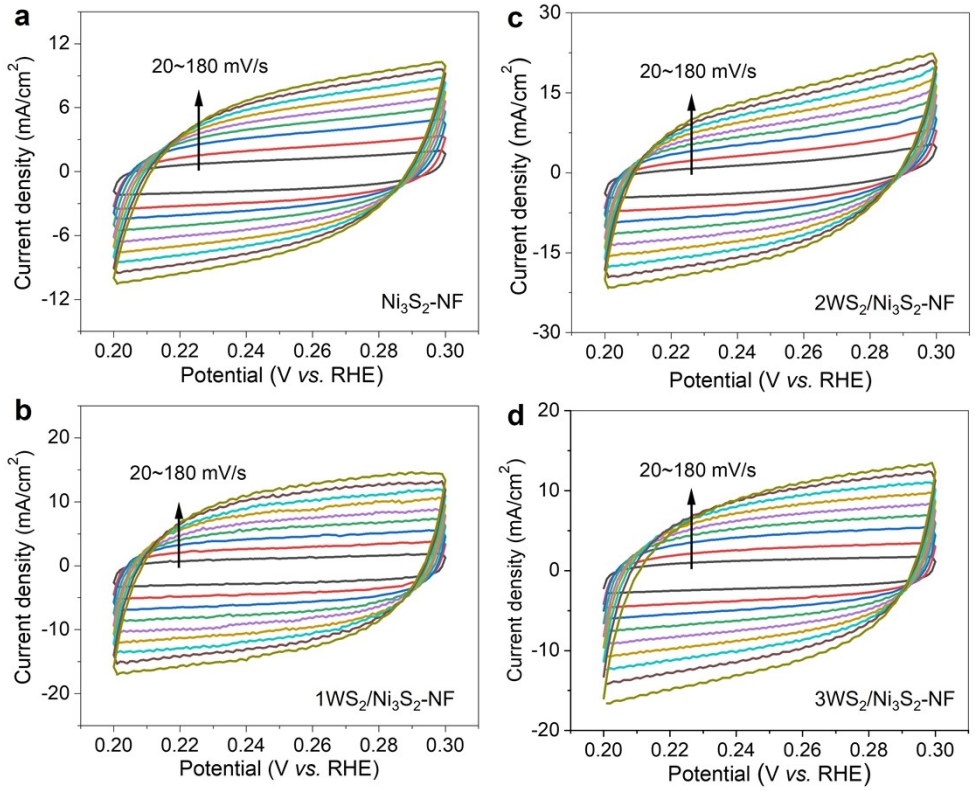

Supplementary Fig. 7 CV curves measured within the range of 0.2 to 0.3 V *vs.* RHE with scan rates from 20 to 180 mV s^{-1} of Ni_3S_2-NF, $1WS_2/Ni_3S_2$-NF, $2WS_2/Ni_3S_2$-NF, $3WS_2/Ni_3S_2$-NF catalysts in 1.0 M KOH solution at 25 ℃.

Supplementary Fig. 8 The photograph of the overall water splitting device. At high current density, it is observed that the electrolytic cell is full of bubbles.

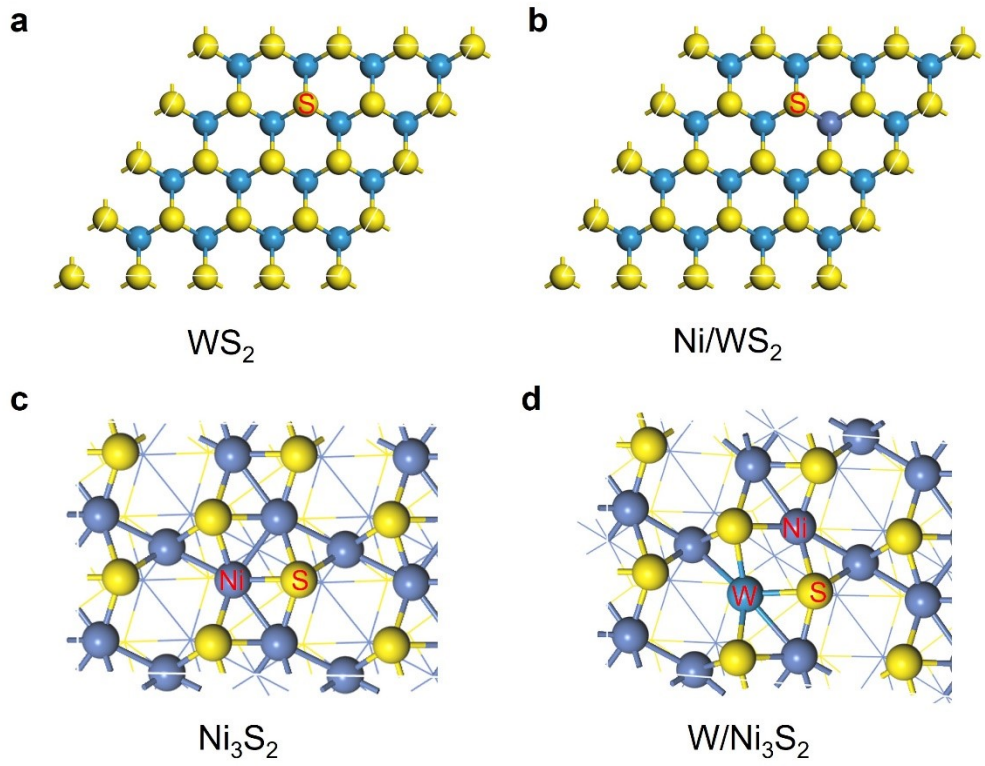

Supplementary Fig. 9 Four optimized surface models, (a) pristine WS_2, (b) Ni-doped WS_2 (Ni/WS_2), (c) pristine Ni_3S_2, and (d) W-doped WS_2 (W/Ni_3S_2) were labeled with different active sites, respectively.

Supplementary Table 1 HER performance of different catalysts in 1.0 M KOH solution at 25 ℃.

Catalysts	Overpotentials (mV *vs.* RHE)				C_{dl} (mF/cm^2)
	η_{100}	η_{500}	η_{1000}	η_{1500}	
Ni_3S_2-NF	267	411	503	575	38.7
$1WS_2/Ni_3S_2$-NF	224	334	402	459	67.7
$2WS_2/Ni_3S_2$-NF	234	317	350	381	78.5
$3WS_2/Ni_3S_2$-NF	220	348	462	571	58.2

Supplementary Table 2 Comparison of HER performance of $2WS_2/Ni_3S_2$-NF with reported WS_2 catalysts.

Catalysts	Electrolyte	η_{100} (mV *vs.* RHE)	η_{1000} (mV *vs.* RHE)	Ref.
$2WS_2/Ni_3S_2$-NF	1 M KOH	234	350	**This work**
V-WS_2/CC	1 M KOH	~260	-	[6]
Co_9S_8/2H-WS_2@NF	1 M KOH	~360	-	[7]
WS/CC	1 M KOH	~610	-	[8]
WS_2TN/CC	1 M KOH	~380	-	[9]
W/WS_2-WC	1 M KOH	~150	473	[10]
WS_2/NiS_x	1 M KOH	~170	-	[11]
Co-$WS_2/NiTe_2$/Ni	1 M KOH	~182	-	[12]
$WS_2@VS_2$	0.5 M H_2SO_4	~240	-	[13]
CeO_2/WS_2/CC	0.5 M H_2SO_4	~200	-	[14]
WS_2NDs	0.5 M H_2SO_4	~270	-	[15]
1T/1T-MWH	0.5 M H_2SO_4	~400	-	[16]

[1] G. Kresse, J. Hafner, Ab initiomolecular-dynamics simulation of the liquid-metal–amorphous-semiconductor transition in germanium, *Phys. Rev. B*, 49 (1994) 14251.
[2] Y. Li, C. Peng, H. Hu, S. Chen, J. Choi, Y. Lin, J. Lee, Interstitial boron-triggered electron-deficient Os aerogels for enhanced pH-universal hydrogen evolution, *Nat. Commun.*, 13 (2022) 1143.
[3] J.K. Nørskov, T. Bligaard, A. Logadottir, J.R. Kitchin, J.G. Chen, S. Pandelov, U. Stimming, Trends in the exchange current for hydrogen evolution, *J. Electrochem. Soc.*, 152 (2005) 23.
[4] S. Grimme, S. Ehrlich, L. Goerigk, Effect of the damping function in dispersion corrected density functional theory, J. Comput. Chem., 32 (2011) 1456.
[5] R.F.W. Bader, Atoms in molecules, *Acc. Chem. Res.*, 18 (1985) 9.
[6] A. Jiang, B. Zhang, Z. Li, G. Jin, J. Hao, Vanadium-doped WS_2 nanosheets grown on carbon cloth as a highly efficient electrocatalyst for the hydrogen evolution reaction, *Chem. Asian J.*, 13 (2018) 1438.
[7] J. Wang, Y. Song, C. Zuo, R. Li, Y. Zhou, Y. Zhang, B. Wu, Y. Huang, An argyrophylla-like nanorods Co_9S_8/2H-WS_2@NF heterojunction with electrons redistribution as a highly efficient bifunctional electrocatalyst for overall water splitting, *ChemCatChem*, 14 (2021) e202101553.
[8] Q. Zhu, W. Chen, H. Cheng, Z. Lu, H. Pan, WS_2 nanosheets with highly-enhanced electrochemical activity by facile control of sulfur vacancies, *ChemCatChem*, 11 (2019) 2667.
[9] M. Liu, A. Geng, J. Yan, Construction of WS_2 triangular nanoplates array for hydrogen evolution reaction over a wide pH range, *Int. J. Hydrogen Energy*, 45 (2020) 2909.
[10] T. Wang, Z. Hong, F. Sun, B. Wang, C. Jian, W. Liu, Interfacial engineering of tungstic disulfide-carbide heterojunction for high-current-density hydrogen evolution, *RSC Adv*, 12 (2022) 27225.
[11] Z. Zhang, X. Lin, S. Tang, Q. Huang, WS_2/NiS_x heterojunction nanosheet clusters: A highly efficient electrocatalyst for hydrogen evolution reaction, *Int. J. Hydrogen Energy*, 47 (2022) 33643.
[12] D.R. Paudel, U.N. Pan, R.B. Ghising, P.P. Dhakal, V.A. Dinh, H. Wang, N.H. Kim, J.H. Lee, Interface modulation induced by the 1T Co-WS_2 shell nanosheet layer at the metallic $NiTe_2$/Ni core-nanoskeleton: Glib electrode-kinetics for HER, OER, and ORR, *Nano Energy*, 102 (2022) 107712.

[13] S. Hussain, D. Vikraman, M. Sarfraz, M. Faizan, S.A. Patil, K.M. Batoo, K.W. Nam, H.S. Kim, J. Jung, Design of XS_2 (X = W or Mo)-decorated VS_2 hybrid nano-architectures with abundant active edge sites for high-rate asymmetric supercapacitors and hydrogen evolution reactions, *Small*, (2022) e2205881.

[14] H. Chen, M. Hu, P. Jing, B. Liu, R. Gao, J. Zhang, Constructing heterostructure of CeO_2/WS_2 to enhance catalytic activity and stability toward hydrogen generation, *J. Power Sources*, 521 (2022) 230948.

[15] X. Zhao, X. Ma, J. Sun, D. Li, X. Yang, Enhanced catalytic activities of surfactant-assisted exfoliated WS_2 nanodots for hydrogen evolution, *ACS Nano*, 10 (2016) 2159.

[16] H. Seok, M. Kim, J. Cho, E. Kim, S. Son, K.-W. Kim, J.K. Kim, P.J. Yoo, M. Kim, H.-U. Kim, T. Kim, Tailoring polymorphic heterostructures of MoS_2-WS_2 (1T/1T, 2H/2H) for efficient hydrogen evolution reaction, *ACS Sustainable Chem. Eng.*, 11 (2023) 568.